Angewandte Chemie
Eine Zeitschrift der Gesellschaft Deutscher Chemiker

Supporting Information

Collective Vibrational Strong Coupling Effects on Molecular Vibrational Relaxation and Energy Transfer: Numerical Insights via Cavity Molecular Dynamics Simulations**

Tao E. Li, Abraham Nitzan,* and Joseph E. Subotnik**

anie_202103920_sm_miscellaneous_information.pdf

Supporting Information for "Collective vibrational strong coupling effects on molecular vibrational relaxation and energy transfer: Numerical insights via cavity molecular dynamics simulations"

Tao E. Li,[1,*] Abraham Nitzan,[1,2,†] and Joseph E. Subotnik[1,‡]

[1] *Department of Chemistry, University of Pennsylvania, Philadelphia, Pennsylvania 19104, USA*
[2] *School of Chemistry, Tel Aviv University, Tel Aviv 69978, Israel*

I. COMPUTATIONAL METHODS

CavMD propagates the following equations of motion for the coupled photon-nuclei system:

$$M_{nj}\ddot{\mathbf{R}}_{nj} = \mathbf{F}^{(0)}_{nj} + \mathbf{F}^{\mathrm{cav}}_{nj}, \tag{S1a}$$

$$m_{k,\lambda}\ddot{\widetilde{q}}_{k,\lambda} = -m_{k,\lambda}\omega^2_{k,\lambda}\widetilde{q}_{k,\lambda} - \widetilde{\varepsilon}_{k,\lambda}\sum_{n=1}^{N_{\mathrm{sub}}} d_{ng,\lambda}. \tag{S1b}$$

Here, subscript nj denotes the j-th nucleus in molecular n, M_{nj}, $\mathbf{R}_{nj}$, $\mathbf{F}^{(0)}_{nj}$, and $\mathbf{F}^{\mathrm{cav}}_{nj}$ denote the mass, position, nuclear force, and cavity force for nucleus nj; see Refs. [S1, S2] for the exact forms of the forces. Subscripts k, λ denote the cavity photon mode with wave vector k and polarization direction $\lambda = x, y$ for a z-oriented cavity (see Fig. 1 for the simulation setup), $m_{k,\lambda}$, $\widetilde{q}_{k,\lambda}$, $\omega_{k,\lambda}$ denote the auxiliary mass, position, and frequency of cavity photon mode k, λ. The cavity photon mode k, λ interacts with the dipole moments of molecules ($d_{ng,\lambda}$) with an effective coupling strength $\widetilde{\varepsilon}_{k,\lambda}$.

A. System size dependence

One important feature of CavMD is the use of periodic boundary conditions. In detail, cavity photons interact with N_{cell} identical simulation cells, each of which contains N_{sub} molecules, so the total molecular number becomes $N = N_{\mathrm{sub}}N_{\mathrm{cell}}$. The replica of N_{cell} simulation cells has been reflected in the definition of

$$\widetilde{\varepsilon}_{k,\lambda} = \sqrt{N_{\mathrm{cell}}}\varepsilon_{k,\lambda} \tag{S2}$$

in Eq. (S1), where $\varepsilon_{k,\lambda}$ is the true coupling strength between a single molecule and the cavity mode k, λ.

When studying how VSC effects can depend on the molecular system size (or the molecular number), we can take $N_{\mathrm{cell}} = 1$ and study the molecular response for different choices of N_{sub} while keeping the molecular density and Rabi splitting the same. Here, the Rabi splitting is unchanged if we modify $\widetilde{\varepsilon}_{k,\lambda}$ according to $\widetilde{\varepsilon}_{k,\lambda} \propto \sqrt{1/N_{\mathrm{sub}}}$. The corresponding CavMD results will reflect the VSC response for a liquid system in cavities with the same polaritonic frequencies but with different effective volumes [S3].

When this system size dependence is studied, according to a second order perturbation calculation, the VSC effect on individual molecules should scale as $O(\widetilde{\varepsilon}^2_{k,\lambda}) = O(1/N_{\mathrm{sub}})$. This $O(1/N_{\mathrm{sub}})$ scaling will quickly remove any VSC effects on individual molecules once N_{sub} is large enough; as has been noted earlier [S4], this approach cannot explain any collective cavity effect.

II. SIMULATION DETAILS

We simulate a model yet realistic molecular system under VSC: the C=O asymmetric stretch mode (peaked at 2327 cm^{-1}) of a large ensemble of liquid-phase CO_2 molecules forms collective VSC with a near resonant cavity mode. The detailed procedure to perform CavMD simulations for such a liquid CO_2 system is given in Ref. [S2] and all input

* taoli@sas.upenn.edu
† anitzan@sas.upenn.edu
‡ subotnik@sas.upenn.edu

files to generate results in this manuscript are available at Github [S5]. Therefore, below we only briefly outline the simulation details.

As shown in Fig. 1, the simulation setup consists of $N_{\rm sub} = 216$ CO_2 molecules in a cubic simulation cell (with cell length 24.292 Å, which corresponds to a molecular density 1.101 g/cm^3) confined within a pair of metallic mirrors along the z-direction. An anharmonic force field [S2] is used to propagate the dynamics of CO_2. During the simulation, only a single cavity photon mode (with two polarization directions: x and y) is considered and the effective coupling strength is set as $\widetilde{\varepsilon} = 2 \times 10^{-4}$ a.u..

We are interested in the cavity modification of both the vibrational energy relaxation of the hot CO_2 molecules and the subsequent intermolecular vibrational energy transfer to the thermal CO_2 molecules. Before simulating this nonequilibrium dynamics, outside a cavity ($\widetilde{\varepsilon} = 0$), we first run 150 ps NVT (constant molecular number, volume, and temperature) simulations at 300 K to equilibrate the system and then run 40 consecutive NVE (constant molecular number, volume, and energy) trajectories with duration 20 ps. Starting from the initial configurations (with both position and velocity information) of the above 40 equilibrium NVE trajectories outside a cavity ($\widetilde{\varepsilon} = 0$), we prepare a nonequilibrium initial condition from equilibrium configurations by resampling the initial velocities of $N_{\rm hot} = 10$ arbitrary CO_2 molecules (in total $N_{\rm sub} = 216$ CO_2 molecules are simulated). The initial conditions of the hot molecules are reset so that their kinetic energy in each degree of freedom obeys a uniform distribution in an interval 6000 ± 250 K. Such a random resampling of velocities has been chosen to mimic the preparation of uncorrelated hot molecules in a thermal bath at room temperature, where the effective temperature of these hot molecules would be ~ 3000 K (since the initial positions of the hot molecules are not modified and still obey a thermal distribution).

Starting from each of the 40 nonequilibrium initial conditions, we then run nonequilibrium NVE simulations for 40 ps and calculate physical properties outside the cavity ($\widetilde{\varepsilon} = 0$) by averaging over the 40 nonequilibrium trajectories. Inside the cavity, we start from exactly the same nonequilibrium initial configurations as the outside cavity case but reset $\widetilde{\varepsilon} = 2 \times 10^{-4}$ a.u. to switch on the light-matter coupling and run NVE trajectories. Note that the use of the NVE ensemble implies that we have neglected any cavity loss, which simplifies the interpretation of results.

III. ON CALCULATING POLARITONIC SPECTRUM

Because polaritons are composed of a molecular bright mode and cavity photons, a polaritonic spectrum can be obtained from either the molecular or the photonic side. From the molecular side, a polaritonic spectrum can be obtained by calculating the molecular infrared (IR) absorption spectrum, which can be evaluated by Fourier transforming the dipole auto-correlation function [S6–S9]:

$$\begin{aligned} n(\omega)\alpha(\omega) = \frac{\pi\beta\omega^2}{2\epsilon_0 V c}\frac{1}{2\pi}\int_{-\infty}^{+\infty} dt\ e^{-i\omega t} \\ \times \left\langle \sum_{i=x,y} \left(\boldsymbol{\mu}_S(0)\cdot\mathbf{e}_i\right)\left(\boldsymbol{\mu}_S(t)\cdot\mathbf{e}_i\right)\right\rangle . \end{aligned} \tag{S3}$$

Here, $\alpha(\omega)$ denotes the absorption coefficient, $n(\omega)$ denotes the refractive index, $\beta = k_{\rm B}T$, V is the volume of the system (i.e., the simulation cell), $\mathbf{e}_i$ denotes the unit vector along direction $i = x, y$, and $\boldsymbol{\mu}_S(t)$ denotes the total dipole moment of the molecules at time t. Fig. 2a and Fig. 3a are calculated by evaluating Eq. (S3) from equilibrium NVE trajectories.

Similar as Eq. (S3), in order to obtain the polaritonic spectrum, we can also define a photonic coordinate auto-correlation function:

$$n(\omega)\alpha_k(\omega) \propto \omega^2 \int_{-\infty}^{+\infty} dt\ e^{-i\omega t} \left\langle \sum_{\lambda=x,y} \widetilde{\widetilde{q}}_{k,\lambda}(0)\widetilde{\widetilde{q}}_{k,\lambda}(t)\right\rangle , \tag{S4}$$

where $\alpha_k(\omega)$ denotes the absorption coefficient for cavity photon mode k. Fig. 5b and Figs. 6b,d are calculated by evaluating Eq. (S4) from nonequilibrium NVE trajectories during the whole simulation period (40 ps). Note that when nonequilibrium trajectories are used to calculate Eq. (S4), the resulting spectrum is a transient spectrum which reflects the average dynamic behavior of photons during the nonequilibrium trajectories.

IV. RABI SPLITTING DEPENDENCE OF VIBRATIONAL RELAXATION BY CHANGING COUPLING STRENGTH

In the manuscript, Fig. 4 shows that the vibrational relaxation of hot molecules is accelerated monotonically as a function of Rabi splitting, where Rabi splitting is enhanced by increasing the isotopic concentration of $^{12}C^{16}O_2$

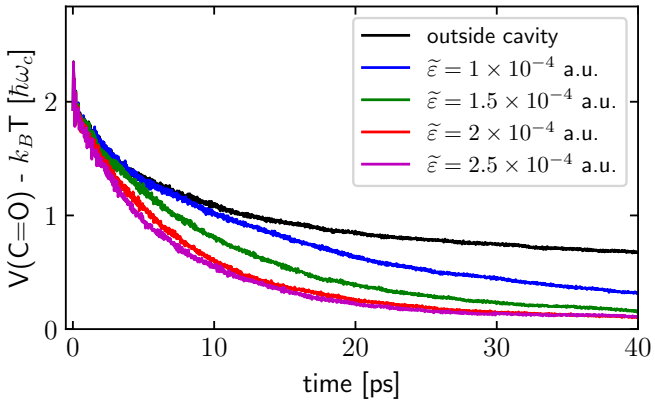

FIG. S1. Average C=O bond potential energy (per molecule) dynamics for the hot molecules outside (black) or inside the cavity under different effective coupling strengths ($\widetilde{\varepsilon}$ spans from 1×10^{-4} to 2.5×10^{-4} a.u.). All the simulation details are the same as Fig. 2b. Note that the vibrational relaxation of the hot molecules is monotonically increased when $\widetilde{\varepsilon}$ (or Rabi splitting) increases, which is similar to Fig. 4b.

molecules. Alternatively, for a given molecular system, Rabi splitting can also be enhanced by simply increasing the effective coupling strength $\widetilde{\varepsilon}$ [S1, S2].

Fig. S1 plots the dynamics for the average C=O bond potential energy of the hot molecules in a pure $^{12}C^{16}O_2$ system under different coupling strengths $\widetilde{\varepsilon}$. When the coupling strength $\widetilde{\varepsilon}$ is increased from 1×10^{-4} (blue) to 2.5×10^{-4} a.u. (magenta), the vibrational relaxation is accelerated monotonically relative to the dynamics outside the cavity (black). Since a larger $\widetilde{\varepsilon}$ corresponds to a larger Rabi splitting [S1, S2], Fig. S1 shows that the vibrational relaxation of hot molecules is accelerated under a larger Rabi splitting, which is very similar to Fig. 4.

V. EFFECT OF CAVITY LOSS

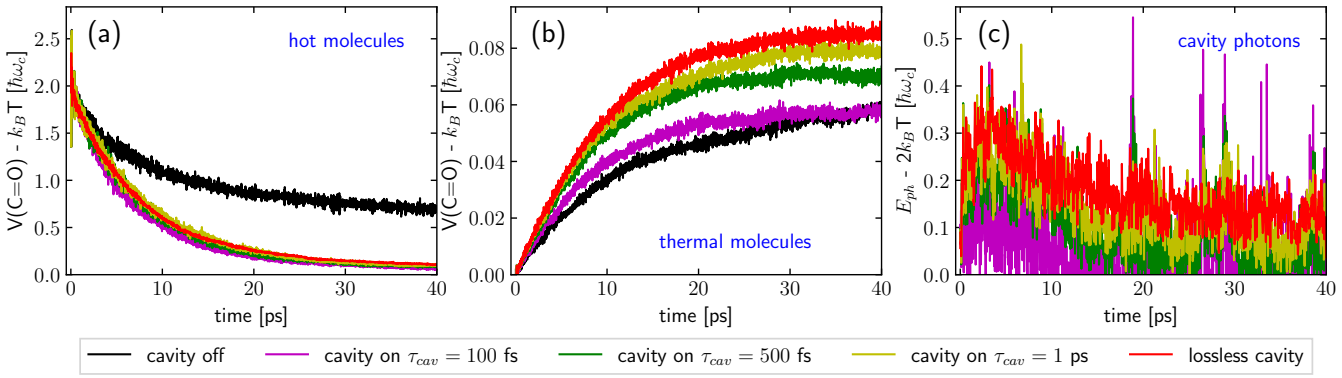

FIG. S2. Effect of cavity loss on vibrational relaxation and energy transfer. Here, we replot Figs. 2b-d in the manuscript. Here, we plot not only results from outside a cavity (black) and inside a lossless cavity (red), but we also plot dynamics inside a lossy cavity when the cavity lifetime is $\tau_{\mathrm{cav}} = 100$ fs (magenta), 500 fs (green), or 1 ps (yellow). Note that including cavity loss does not meaningfully modify vibrational relaxation of the hot molecules (see Fig. a) but can meaningfully suppress vibrational energy transfer to thermal molecules once the cavity lifetime is shorter than 1 ps (see Fig. b).

The results presented in the manuscript assume a perfect or lossless cavity. In realistic experiments, however, cavity loss is inevitable. We have argued (in manuscript) that, in Fabry–Pérot microcavities, cavity loss should not meaningfully alter the polaritonic effect on vibrational relaxation and energy transfer. Because VSC can also form in plasmonic cavities (which has a large cavity loss), it is crucial to investigate whether or not increasing cavity loss can significantly modify the results in the manuscript.

Within the framework of CavMD, we introduce cavity loss by coupling only the momenta of cavity photons to a Langevin thermostat. The friction lifetime of the Langevin thermostat defines the cavity lifetime τ_{cav} (or the inverse

of the cavity loss rate).

Following up on Fig. 2 in the main text, we have rerun all nonequilibrium CavMD simulations with cavity loss included. Fig. S2 plots the dynamics of (a,b) the average C=O bond potential energy for each hot molecule and thermal molecule, as well as (c) the total energy of cavity photons. Apart from the results for outside a cavity (black) and inside a lossless cavity (red) which are identical to Figs. 2b-d, dynamics for different cavity lifetimes are also given: $\tau_{\rm cav}$ = 100 fs (magenta), 500 fs (green), and 1 ps (green). As shown in Fig. S2a, including cavity loss does not meaningfully alter the vibrational relaxation dynamics of the hot molecules. By contrast, cavity loss does modify vibrational energy transfer to the thermal molecules (see Fig. S2b): When $\tau_{\rm cav}$ = 100 fs (magenta), the energy transfer dynamics largely reduces to the outside-cavity result; when $\tau_{\rm cav}$ = 1 ps (yellow), the energy transfer dynamics is only weakly suppressed compared with the lossless cavity result. As far as the dynamics for the cavity photons are concerned (Fig. S2c), increasing cavity loss suppresses the initial transient excitation of the photons but also enhances the fluctuations of the signals.

From Fig. S2, we can conclude that once the cavity lifetime exceeds 1 ps (e.g., in Fabry–Pérot microcavities [S10]), the conclusions in the manuscript should hold perfectly. While in general cavity loss does not meaningfully modify the vibrational relaxation of hot molecules, a very lossy cavity ($\tau_{\rm cav}$ = 100 fs) can completely remove the cavity effect on energy transfer because, in this limit, cavity photons leak out the cavity and do not transfer energy meaningfully to the thermal molecules.

VI. EFFECT OF TEMPERATURE OF HOT MOLECULES

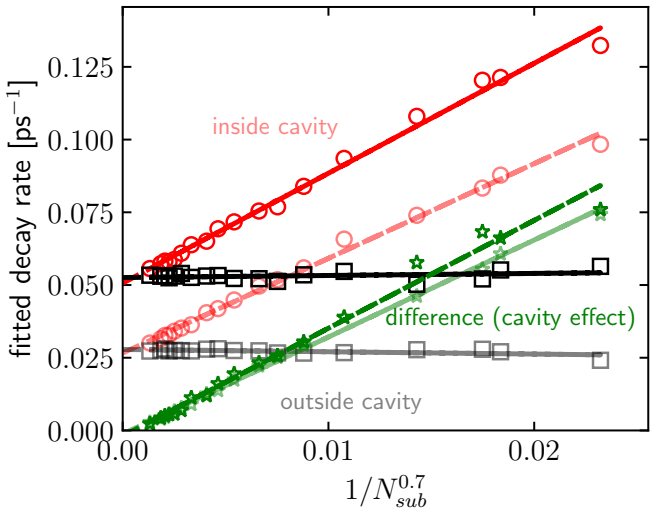

FIG. S3. Vibrational relaxation rates of the hot molecules versus the system size ($N_{\rm sub}$) when the hot molecules start with different initial kinetic energies. The rates for hot molecules starting with a 6×10^3 K kinetic energy (light-colored lines) is a replot of Fig. 6c: light-red circles denote the inside-cavity rates, light-black squares denote the outside-cavity rates, and light-green stars denote the pure cavity effect (difference between the inside- and outside-cavity rates). The deep-colored lines denote the relaxation rates when the hot molecules start with a 1.2×10^4 K kinetic energy and all the other parameters are the same as Fig. 6c. Note that increasing the kinetic energy by a factor of two does not meaningfully alter the cavity effects on relaxation rates.

[S1] T. E. Li, J. E. Subotnik, and A. Nitzan, Proc. Natl. Acad. Sci. **117**, 18324 (2020), arXiv:2004.04888.
[S2] T. E. Li, A. Nitzan, and J. E. Subotnik, J. Chem. Phys. **154**, 094124 (2021), arXiv:2011.03192.
[S3] Note that periodic boundary conditions are always applied to exclude the edge effect of the simulation cell.
[S4] P. Pilar, D. De Bernardis, and P. Rabl, Quantum **4**, 335 (2020), arXiv:2003.11556v5.
[S5] T. E. Li, "Cavity Molecular Dynamics Simulations Tool Sets," https://github.com/TaoELi/cavity-md-ipi (2020).
[S6] D. A. McQuarrie, *Statistical Mechanics* (Harper-Collins Publish- ers, New York, 1976).
[S7] M.-P. Gaigeot and M. Sprik, J. Phys. Chem. B **107**, 10344 (2003).
[S8] S. Habershon, G. S. Fanourgakis, and D. E. Manolopoulos, J. Chem. Phys. **129**, 074501 (2008).

[S9] A. Nitzan, *Chemical Dynamics in Condensed Phases: Relaxation, Transfer and Reactions in Condensed Molecular Systems* (Oxford University Press, New York, 2006).

[S10] B. Xiang, R. F. Ribeiro, M. Du, L. Chen, Z. Yang, J. Wang, J. Yuen-Zhou, and W. Xiong, Science (80-.). **368**, 665 (2020).